JOURNAL OF AIRCRAFT
Vol. 45, No. 4, July–August 2008

Nose Blowing for Side Force Control on Slender Cones at High Incidence

Rajan Kumar* and P. R. Viswanath†
National Aerospace Laboratories, Bangalore 560 017, India
and
O. N. Ramesh‡
Indian Institute of Science, Bangalore 560 012, India

DOI: 10.2514/1.33748

Vortex asymmetry on axisymmetric pointed forebodies at high angles of incidence results in side forces and adverse yawing moments even in symmetric flight. An experimental investigation has been carried out at low speeds to study the effectiveness of axial nose blowing against the oncoming flow for side force control on two slender cones. Tests were made on the 8 and 12 deg cone models with (circular) jet flow over a Reynolds number range of 0.4×10^6 to 5.4×10^6. Jet-to-freestream velocity ratio was varied up to 2.0, and the blowing diameter was varied as well. Force measurements were carried over the incidence range of 0 to 45 deg, and limited surface pressure distributions were obtained on the 12 deg cone model. The results explicitly show the effectiveness of nose blowing for side force control over a wide range of Reynolds numbers, and minimum side force was reached around a jet velocity ratio of 1.0. An important result is that the side force reduction correlates with jet velocity ratio in the range of parameters studied. Broad similarities in the trend of side force reduction with the nose blowing and the nose bluntness suggest that the interaction of axial jet with freestream flow results, possibly, in what we may call "fluid dynamic blunting."

Nomenclature

A_b	=	cone base area, $\pi/4\ D^2$
A_J	=	jet area, $\pi/4\ d_J^2$
C_m	=	jet mass flow ratio, m_J/m_∞
C_N	=	normal force coefficient, normal force$/q_\infty A_b$
C_P	=	static pressure coefficient, $(p - p_\infty)/q_\infty$
C_S	=	side force coefficient, side force$/q_\infty A_b$
$C\mu$	=	jet momentum ratio, $m_J U_J/m_\infty U_\infty$
D	=	cone base diameter (=160 mm)
d_J	=	jet diameter
M_∞	=	freestream Mach number
m_J	=	jet mass flow rate, $\rho_J U_J A_J$
m_∞	=	reference mass flow rate, $\rho_\infty U_\infty A_b$
p	=	local static pressure
p_J	=	jet pressure
p_∞	=	freestream static pressure
q_∞	=	freestream dynamic pressure
Re_D	=	Reynolds number based on base diameter, $\rho_\infty U_\infty D/\mu$
r_N	=	nose radius
U_J	=	jet velocity
U_∞	=	freestream velocity
V_J	=	volumetric flow rate of jet
U_J/U_∞	=	jet velocity ratio
α	=	angle of incidence, deg
α_o	=	angle of incidence corresponding to vortex asymmetry onset, deg
ΔC_N	=	uncertainty in normal force coefficient
ΔC_P	=	uncertainty in static pressure coefficient
ΔC_S	=	uncertainty in side force coefficient
θ_C	=	semi-apex cone angle, deg
ρ_J	=	jet flow density
ρ_∞	=	freestream density
ϕ	=	circumferential angle, deg
ψ	=	roll position, deg
$2r_N/D$	=	bluntness ratio

Received 27 July 2007; revision received 4 February 2008; accepted for publication 5 February 2008.

*Scientist, National Trisonic Aerodynamic Facilities; currently Research Scientist, Advanced Aero-Propulsion Laboratories, Florida State University, Tallahassee, FL 32310. Member AIAA.
†Head, Experimental Aerodynamics Division. Associate Fellow AIAA.
‡Assistant Professor, Department of Aerospace Engineering.

I. Introduction

MODERN fighter aircraft and missiles are expected to perform post-stall maneuverability to achieve tactical advantages. This can result in flight at high angles of attack (up to 45–50 deg) and knowledge of the nonlinear aerodynamics, including strong viscous effects leading to crossflow separation, becomes very important in the design of a flight vehicle. One of the important problems, which has received considerable attention (e.g., Hunt [1], Ericsson and Reding [2], Champigny [3], and Williams [4]) during the last two decades, is the phenomenon of vortex asymmetry on pointed forebodies at high angles of attack and the resulting side forces and adverse yawing moments, even in symmetric flight (zero side slip): the yawing moments generated are often too large to be controlled by using the rudder power in the case of a fighter aircraft. The major geometric parameters that are known to influence vortex asymmetry include nose apex angle, forebody cross-sectional shape, and fineness ratio of the slender body. The side forces generated are strongly Reynolds number dependent, and the effects gradually decrease with increase in flight Mach number; the problem is essentially predominant at low to subsonic speeds in which high alpha maneuvers normally occur.

Because the adverse yawing moments can be very large and also difficult to predict even in an engineering sense, there have been several attempts to reduce or even alleviate these undesirable side forces by both passive and active flow control techniques. These include different kinds of nose strakes [5–9], boundary layer trips [6,10,11], nose blunting [6,12,13], and nose tip rotation [14], and the beneficial effects of many of the previously mentioned devices have been demonstrated over a limited range of flow parameters like Mach number and Reynolds number. Recently, Rajan Kumar et al.[15] carried out a systematic parametric study of nose bluntness on two slender cones for side force control covering a wide range of

Reynolds numbers: many interesting features of vortex asymmetry and side force generated were brought out.

There have been several investigations exploring the asymmetric vortex flow behavior on slender bodies at high angles of attack and active methodologies for controlling the same. Williams and Papazian [16] used an unsteady bleed technique through a number of holes in the nose region for forebody vortex control at low speeds; the bleed momentum was varied at a fixed forcing frequency. Using smoke-flow visualization studies and one-component laser Doppler velocimetry (LDV) measurements, they showed that unsteady bleed was effective in symmetrizing the naturally occurring asymmetric vortex flow at $\alpha = 55$ deg. In a later study, Bernhardt and Williams [17] investigated the response of the side force to controlled forcing using steady suction and bleed. The experiments were made on a slender body model over a range of Reynolds numbers (based on D) of 6.3×10^3–8.01×10^4; two independent sets of suction/bleed holes were located at ± 135 deg (with respect to the windward plane) and very close to the tip of the model. Based on LDV velocity measurements in the nose region, they suggested that the response of the vortex system to forcing was Reynolds number dependent, and further, both suction and blowing were capable of controlling symmetry of flows on pointed forebodies. Subsequently, Bernhardt and Williams [18] employed an unsteady bleed technique (in the nose region of a long slender body) to demonstrate control of asymmetry as well as generate side force and yawing moments that can be used to enhance the maneuverability at high alpha; these experiments were carried out at a Reynolds number of 6.3×10^3 and $\alpha = 45$ and 55 deg. The mean velocity profiles measured in the nose region (downstream of the nose tip) were analyzed from the point of view of the stability of the vortex system. They suggested that the source of asymmetric flow up to $\alpha = 45$ deg is convective instability, and at $\alpha = 55$ deg is a global instability mechanism. The origin and the behavior of the asymmetric vortex flow were further investigated experimentally by Degani and Tobak [19]. They used a thin (0.5 mm in diameter) wire as a protuberance near the nose tip of a tangent ogive cone cylinder to generate a controlled flow asymmetry. Their results showed the presence of convective instability over the entire alpha range tested (up to 60 deg) in contrast to the idea of global instability at angles of attack beyond 50 deg, reported earlier [18].

There have been other studies [20–23] devoted to generating asymmetry of the forebody vortex system for obtaining yaw control at high alpha. Roos and Magness [22] used a blunted nose (bluntness ratio = 20%) and a pair of small jets at ± 135 deg from the stagnation line on an ogive cylinder model to control the forebody vortex asymmetry. Their results show that the side force coefficient scaled with the mass flow coefficient over a Reynolds number range of 0.7×10^5 to 2.2×10^5. In another study, Roos [23] made a comparison of microblowing with conventional nozzle blowing, and found that microblowing is more effective at very high angles of attack ($55 < \alpha < 70$ deg), whereas conventional surface nozzle blowing was effective at moderate angles of attack, that is, $30 < \alpha < 55$ deg. An excellent review on the subject has been written by Malcolm [24].

In this paper, we have investigated in some detail the effectiveness of axial nose blowing against the oncoming flow as an active control method to alleviate/reduce side forces on slender cones at high angles of attack. Such a technique has not been explored for side force control in literature. The experiments were carried out on two cone models with semi-apex angles of 8 and 12 deg over a wide range of Re_D (0.4×10^6 to 5.4×10^6). Force/moment measurements have been made using a strain gauge balance, and the effectiveness of nose blowing for side force control has been demonstrated. The results are discussed both from the point of view of vortex asymmetry onset and side force characteristics. Broad similarities in the results of axial nose blowing with those due to nose blunting having been noted.

II. Experiments

A. Test Facilities

A major part of the experiments involving balance and surface pressure measurements at the lowest freestream velocity (40 m/s) were carried out in the National Aerospace Laboratories (India) (NAL) 1.5×1.5 m low turbulence low speed wind tunnel, in which the freestream velocity can be regulated within 1% and the freestream turbulence level is very low (<0.12%). Limited experiments were carried out in the NAL 1.2×1.2 m trisonic wind tunnel (with solid walls) to take advantage of a wide range of Reynolds numbers possible in the facility by varying both freestream Mach number and tunnel stagnation pressure. In both facilities, the incidence range of 0–45 deg was carried out by employing a high alpha attachment integrated to the main pitch system.

B. Test Models

Experiments were made on two cone models with semi-apex angles of the 8 and 12 deg, which had provision for introducing an axisymmetric jet flow at the nose tip; for these experiments, the baseline cone model (namely without blowing) was mildly blunted ($2r_N/D = 2\%$) to ensure coaxial jet flow, which was considered very important (otherwise the jet flow can lead to asymmetric effects). The geometrical details of the cone models used on these tests are given in Fig. 1. Each cone model was made in two sections: the front nose portion with 2% bluntness and the rear (cone-frustum) portion, which was the same for a given cone model. The jet diameter d_J on each cone model was varied by choosing two separate nose sections with 0.5- and 1.0-mm-diam holes drilled coaxially with great care. These nose sections were also used as 2% blunted cone models (as a baseline for comparison with jet blowing later) by closing the holes with wax using great care. This procedure enabled maintaining the same roll sensitivity for the blunted cone and with nose blowing as there was provision to roll the front nose portion at 45 deg interval for assessing the roll sensitivity.

Surface pressure measurements were made only on the 12 deg cone models as shown in Fig. 2. A cone frustrum section with pressure ports was fabricated, and the two nose sections with $d_J =$ 0.5 and 1.0 mm (used with force/moment model) were fitted on to it. This facilitated maintaining the same roll sensitivity for both aerodynamic load as well as pressure measurements. The model had two rows of static pressure taps (30 nos. each at S1 and S2 stations) as shown in Fig. 2.

C. Instrumentation and Measurements

1) Force and moment measurements were made on both the 8 and 12 deg cone models with and without nose blowing. These were made using two separate internal strain gauge balances of appropriate range for tests in the 1.2 and 1.5 m wind tunnels so that data accuracy is maintained. The load ranges for 38.1 mm (1.5 in.), six-component strain gauge balance used in 1.2 m wind tunnel were normal force = 545 kg, side force = 273 kg, axial force = 27 kg, pitching moment = 42 kg · m, yawing moment = 17 kg · m, and rolling moment = 4.62 kg · m. The load ranges for the five-component balance used in 1.5 m low speed tunnel were normal force = 8 kg, side force = 4 kg, pitching moment = 0.9 kg · m, yawing moment = 0.45 kg · m, and rolling moment = 0.05 kg · m. The measurement accuracy of strain gauge balances used in the 1.2 m trisonic wind tunnel and 1.5 m low speed wind tunnel are $\pm 0.1\%$ and $\pm 1.0\%$ of full capacity, respectively. Balance measurements were made with nose blowing at a fixed value of U_J covering an incidence range of 0–45 deg in pitch and pause mode, and this procedure was repeated at other values of jet velocity U_J. Measurements for the no-blowing case ($U_J = 0$) were carried out by carefully plugging the nose holes with wax.

2) The static pressure distributions on the 12 cone model (Fig. 2) were measured both with and without nose blowing at a freestream velocity of 40 m/s. All the static pressure ports were connected to two units of 32-port electronically scanned pressure (ESP) scanners having a range of ± 254 mm of water. The ESP scanners were accurately calibrated before use.

3) The volumetric flow rate V_J of the jet flow was measured using a rotameter in the circuit. A schematic of the instrumentation used to calculate the jet velocity is shown in Fig. 3. As the mass flow

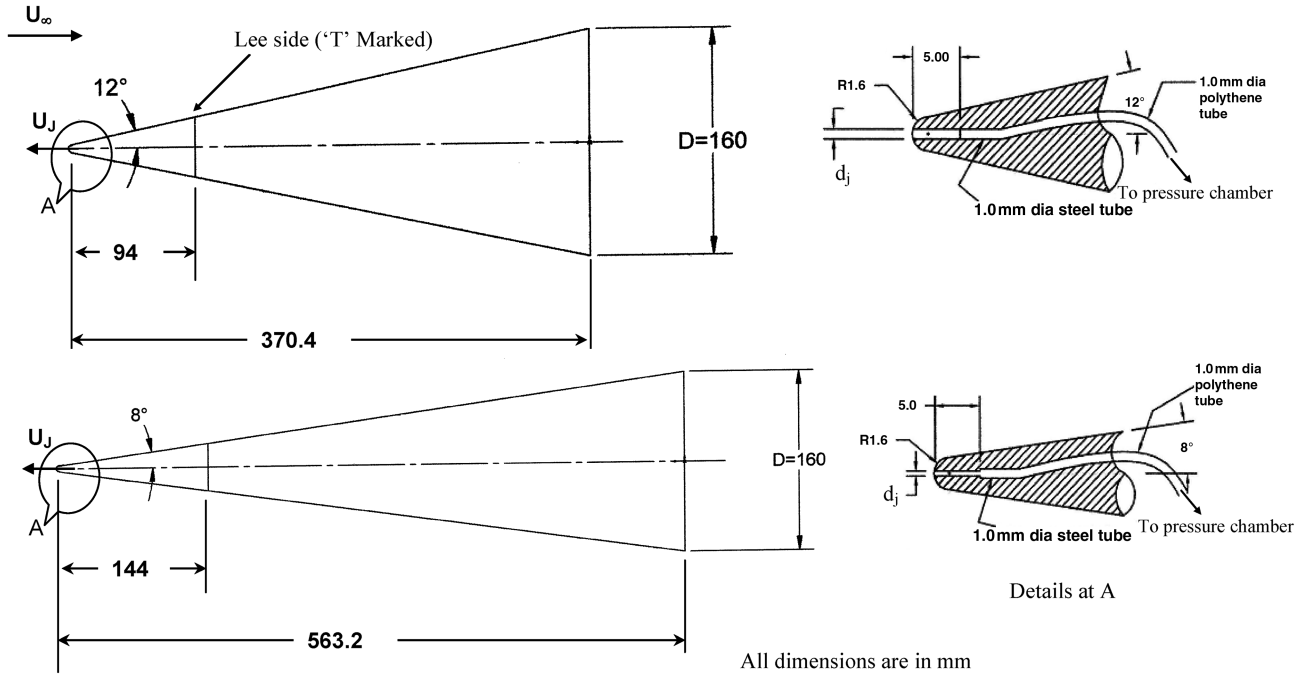

Fig. 1 Geometrical details of blunted ($2r_N/D = 2\%$) cone models with jet flow.

involved in present studies was very small, the rotameters used for these tests were of low range (20–200 and 30–300 l/h). With cone model present in the circuit (with different nose sections), the variation of volumetric flow rate V_J (rotameter reading) as dependent on the settling chamber jet total pressure P_J (read by the pressure gauge) was first established (see [25]). The jet velocity was calculated from the volumetric flow rate measured by the rotameter; this exercise was carried out over the range of jet velocity required for the present series of experiments. The jet velocity so calculated was checked against velocity measured using a constant temperature hotwire system, and an excellent agreement was found within $\pm 1\%$ (see [25]). More details on the instrumentation used to measure jet velocity and their calibration are given in [25]. Provision was made to switch on and off the jet flow as needed.

4) Limited surface flow visualization studies using titanium dioxide in oleic acid and vacuum oil were carried out on the 12 deg cone model with $d_J = 1.0$ mm; these were done only at selected flow conditions.

The balance measurements in the 1.5 m tunnel were carried out in a pitch and pause mode in steps of 2 deg at a sampling rate of 50 samples/s for a time period of 10 s. In the 1.2 m tunnel, data was obtained at continuous pitch mode at a slow rate of 2 deg/s with a sampling frequency of 275 Hz; it was ascertained that side force generated in the continuous pitch and pitch/pause mode were virtually the same. The balance and transducer output signals were acquired on a PC-based data acquisition system and processed offline on a computer.

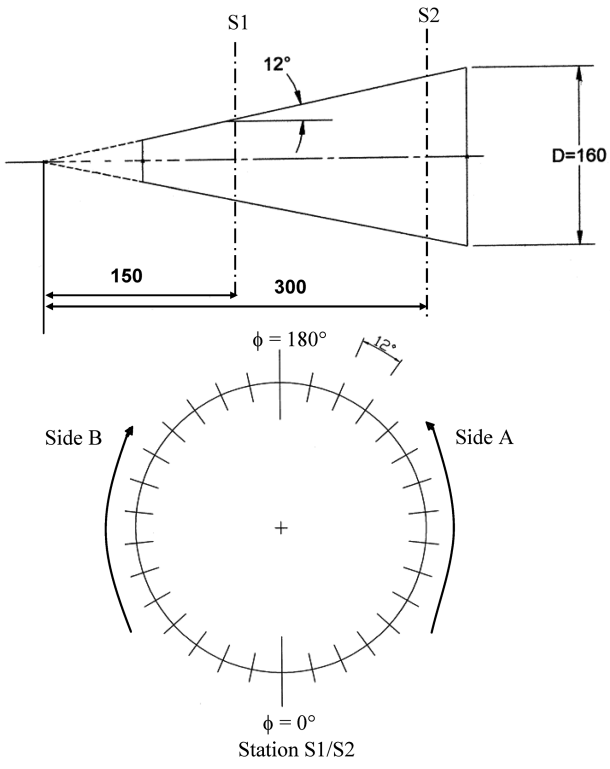

Fig. 2 Geometrical details of 12 deg cone pressure model.

D. Test Conditions

Most detailed measurements on both the cone models were carried out in the 1.5 m low speed wind tunnel at a freestream velocity of 40 m/s and the corresponding Reynolds number based on base diameter Re_D was 0.4×10^6. Tests in the 1.2 m tunnel were carried out at two higher Reynolds numbers (Re_D) of 0.9×10^6 and 5.4×10^6. These were obtained by operating the tunnel at Mach numbers 0.17 and 0.40 and at the tunnel stagnation pressure of 138 kN/m^2 (20 psi) and 414 kN/m^2 (60 psi). These experiments were conducted to establish the effectiveness of nose blowing for side force control at relatively higher Reynolds numbers of relevance in design applications. The test conditions and associated measurements are summarized in a Table 1.

E. Measurement Uncertainties

The accuracy of the measured force and moment coefficients depends on the individual accuracy of various measuring instruments used and the flow parameters. The strain gauge balances and pressure transducers were accurately calibrated before use in the present experimental program. As mentioned earlier in Sec. III, the measurement accuracy of strain gauge balances used in the 1.2 m trisonic wind tunnel and 1.5 m low speed wind tunnel are $\pm 0.1\%$ and

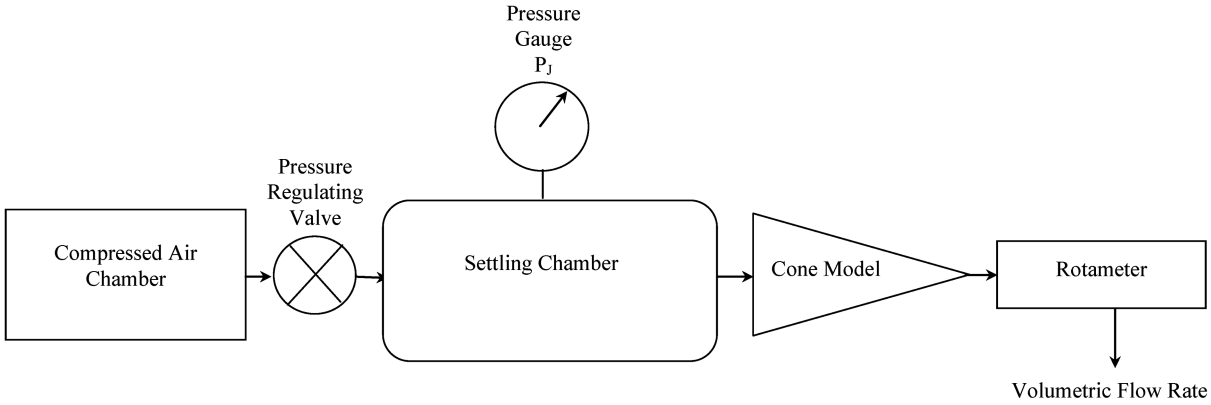

Fig. 3 Schematic of the instrumentation used to measure volumetric flow rate.

$\pm 1.0\%$ of full capacity, respectively. It may be noted that the balance used for measurements in the 1.5 m low speed tunnel was of much lower capacity than the one used in the 1.2 m wind tunnel. Considering the levels of maximum side force measured in the two tunnels, the inaccuracies in side force measurement in both the tunnels were nearly the same. The uncertainty obtained by static calibration of pressure transducers is $\pm 0.5\%$ of full scale. The uncertainty in the measurement of jet velocity includes measurement accuracy of rotameters, pressure regulating valve, and pressure measurement gauge. The pressure was regulated well within ± 1.7 kN/m^2 (0.25 psi). The rotameters used for these tests were carefully calibrated (see [25]); taking into account the repeatability, the uncertainty in the measurement of jet velocity is estimated to be less than 1 m/s. Based on the method suggested by Kline and McClintock [26] and taking account of repeatability tests, estimates of maximum measurement uncertainty were: normal force coefficient, $\Delta C_N \leq \pm 0.02 C_N$ (20 to 1), side force coefficient, $\Delta C_S \leq \pm 0.02 C_S$ (20 to 1), and static pressure coefficient, $\Delta C_p \leq \pm 0.015 C_p$ (20 to 1).

Because we were dealing with a new concept involving nose blowing for side force control, limited tests were made to examine any hysterisis effects on the results. Tests were made on the two cone models: 1) with nose blowing turned on at any desired value and the model pitched to various angles of attack, and 2) with the model pitched to a relatively high α, generating a side force, and then the jet flow was turned on at a desired U_J. It was found from these experiments that the effectiveness of side force control was practically the same (within the accuracy of side force measurements) for both the cone models indicating absence of any hysterisis. For more details, see [25].

III. Results and Discussions

A. General

The focus of the present study being on side force generated and its control using axial nose blowing, results of side force characteristics from all the tests made on both the cone models are presented here. This will be followed by results of surface pressure distributions and surface flow visualization studies for selected models and test conditions. For completeness, limited results on normal force characteristics are included as well. As indicated earlier, detailed balance and pressure measurements were carried out at a $Re_D = 0.4 \times 10^6$, and the jet velocity ratio was systematically varied over a range of 0 to 2.0. Certain major observations will be discussed based on these results. Results from the high Reynolds number tests will be presented essentially to demonstrate the effectiveness of blowing relevant to practical applications.

The side force and normal force are nondimensionalized by the freestream dynamic pressure q_∞ and reference base area A_b. Jet velocity U_J is nondimensionalized by the freestream velocity U_∞. Vortex asymmetry onset α_o was identified as the angle of attack for which the side force coefficient C_S generated had a small value of 0.02; this value was chosen because the balance system used could resolve side force coefficient to this accuracy reliably.

B. Roll Sensitivity Tests

In the context of studies on vortex asymmetry on slender bodies at high angles of attack, it is useful and appropriate to recall the importance of "roll search" and determination of "stable roll position" for each configuration (Hunt [1]). Stable roll is generally defined as the roll position corresponding to which the side force is maximum and insensitive to small changes in roll angle. In literature, typically no more than four to eight roll positions are tested for roll sensitivity due to practical difficulties. In the present study, roll sensitivity tests were made on the 2% blunted cone models with holes in the nose section smoothly plugged with wax; as a result, the roll sensitivity was maintained on a given cone with and without jet blowing. Stable roll was determined for all the four cone model configurations (two nose sections on each cone model) at eight roll positions (45 deg apart) covering 360 deg at $Re_D = 0.4 \times 10^6$ corresponding to maximum side force levels generated. Stable roll position can be determined by either rotating the nose section or the entire body, because the phenomenon of vortex asymmetry is essentially nose triggered [1,6]. Here we have rotated the nose section because it was very convenient because the model was made in two sections (Fig. 1). With reference to Fig. 1, roll position is defined as the roll angle ψ measured with respect to the leeside (top)

Table 1 Test conditions

Model configuration		Type of measurement	Test conditions	
Cone angle, θ_c	Jet diameter, d_J		Freestream velocity, U_∞ Mach number, M	Reynolds number, Re_D
8, 12 deg	0.5	Force and moment	40 m/s	0.4×10^6
8, 12 deg	1.0	Force and moment	40 m/s	0.4×10^6
8, 12 deg	1.0	Force and moment	0.17[a]	0.9×10^6
8, 12 deg	1.0	Force and moment	0.40[a]	5.4×10^6
12 deg	0.5, 1.0	Pressure measurements	40 m/s	0.4×10^6
12 deg	1.0	Surface flow visualization	40 m/s	0.4×10^6

[a]Tests made in the 1.2 m tunnel.

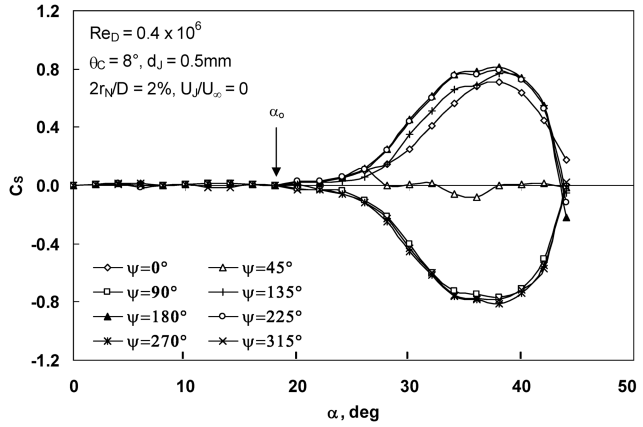

a)

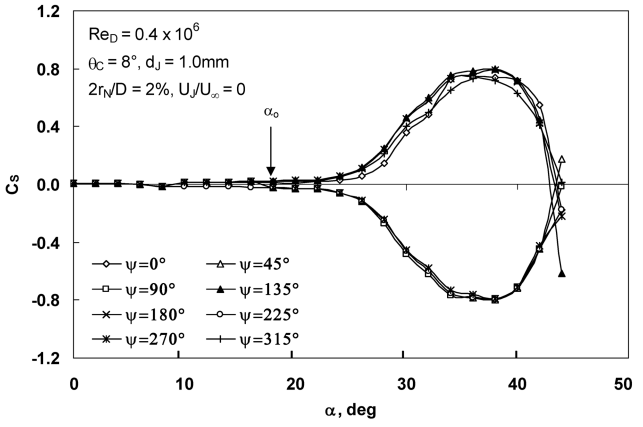

b)

Fig. 4 Variation of side force with roll position for 8 deg cone models.

generator in the pitch plane. Side force variations on the 8 deg cone model with $d_J = 0.5$ and 1.0 mm at eight roll positions are shown in Fig. 4. Based on these results, $\psi = 180$ deg and $\psi = 135$ deg were chosen as stable roll positions for 8 deg cones with $d_J = 0.5$ and 1.0 mm, respectively: these roll positions correspond to maximum side force levels generated. Alternatively, $\psi = 225$ deg and $\psi = 180$ deg could have been chosen as well, as the maximum side force levels generated for these roll positions were nearly the same as those for the roll positions already chosen previously. Similarly, stable roll positions for 12 deg cone models were also determined (not shown here), and all the side force characteristics on different models were obtained at the stable roll position chosen previously.

C. Broad Features of Vortex Asymmetry Onset and Side Force Characteristics with Nose Blowing

We present here typical results of vortex asymmetry onset and side force characteristics on both the cone models obtained at a Reynolds number of 4×10^6; the results on the 12 deg cone are presented in Figs. 5 and 6 and those on the 8 deg cone in Figs. 7 and 8. It may be noted that each figure contains side force data at different values of the velocity ratio, U_J/U_∞; the values of vortex asymmetry onset (α_o) inferred as dependent on U_J/U_∞ are also included in each figure. The α_o values could be generally inferred to an accuracy of ± 1 deg from the side force data. Results of α_o and side force corresponding to no blowing condition ($U_J/U_\infty = 0$), namely, on the 2% blunted cone model, are also included in all the figures for comparison. It is interesting to observe from Figs. 5–8 that axial nose blowing is generally effective in the reduction of side forces depending on the magnitude of the jet velocity ratio; on the 12 deg cone, side force reduction is as high as 70–80% at $U_J/U_\infty = 1.0$. Associated with the side force reduction, there is delay in the vortex asymmetry onset α_o, which is to be expected. Detailed observations on the effectiveness of blowing are summarized below.

In the absence of blowing ($U_J/U_\infty = 0$), the α_o values are slightly higher than $2\theta_C$ ($\alpha_o = 2\theta_C$, a well-known feature of pointed forebodies [1,15]), which is to be expected because of mild nose blunting of 2%. The following general trend of vortex asymmetry onset with the jet velocity ratio is seen on both the cone models; α_o increases initially with U_J/U_∞, followed by a small decrease and then a gradual increase for large values of U_J/U_∞. For example, on the 12 deg cone with $d_J = 1.0$ mm (Fig. 6), α_o increases from 26 deg (no jet flow) to about 38 deg at $U_J/U_\infty = 0.99$, followed by a decrease to 36 deg at $U_J/U_\infty = 1.12$ and 1.23 and then small increase to 38 deg for higher velocity ratios. An extremely similar trend is observed for the cone with $d_J = 0.5$ mm as well (Fig. 5) and we shall discuss other aspects of vortex asymmetry onset later.

Associated with the observed trend of α_o with U_J/U_∞ discussed previously, there is a corresponding trend in the absolute value of maximum side force generated as well, which may be inferred from the results (Figs. 5 and 6); an increase in α_o is associated with a decrease in side force level and vice versa. For example, on the 12 deg cone with $d_J = 1.0$ mm (Fig. 6), maximum side force magnitude decreases from 0.68 at $U_J/U_\infty = 0$ to a relatively low level about 0.12 at a velocity ratio of 0.99, then a small increase for $U_J/U_\infty = 1.11$ and eventual decrease for higher velocity ratios. This trend of maximum side force variation with velocity ratio is to be

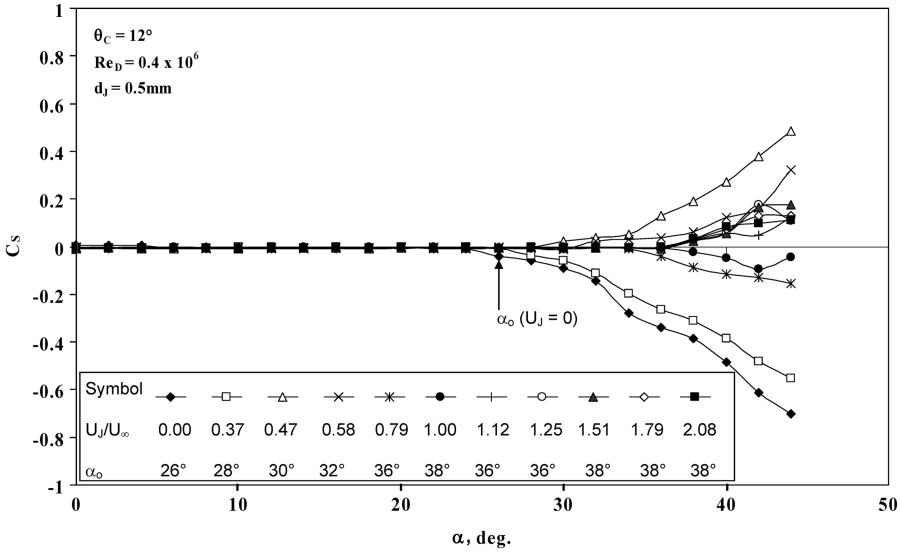

Fig. 5 Side force characteristics on 12 deg cone with nose blowing.

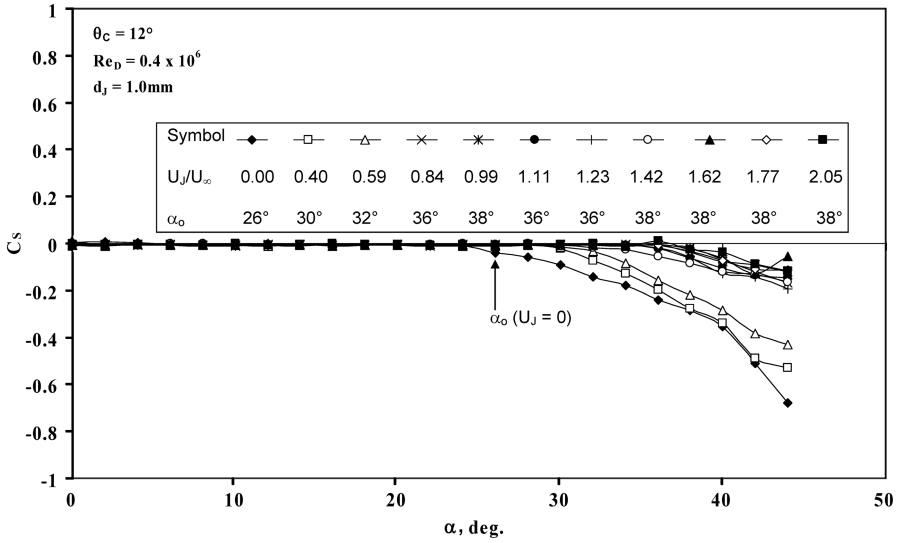

Fig. 6 Side force characteristics on 12 deg cone with nose blowing.

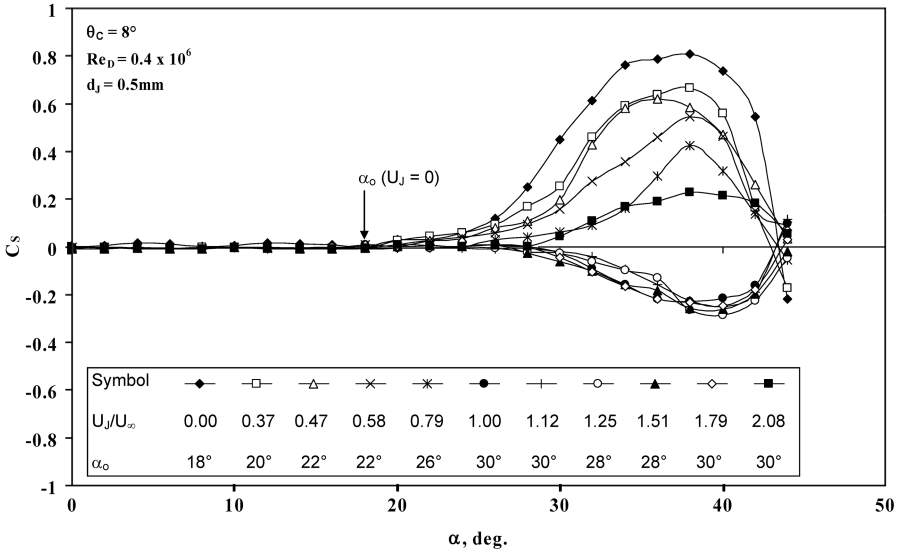

Fig. 7 Side force characteristics on 8 deg cone with nose blowing.

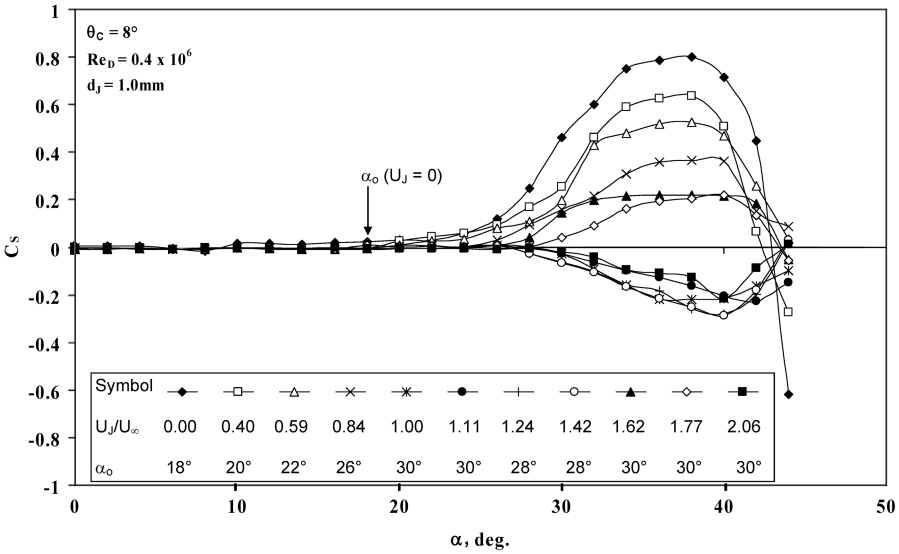

Fig. 8 Side force characteristics on 8 deg cone with nose blowing.

expected, because a delay in vortex asymmetry onset will (normally) result in decrease in maximum side force levels generated. Such a qualitative trend of side force characteristics with jet velocity ratio is also observed on the 12 deg cone with $d_J = 0.5$ mm as well (Fig. 5).

The results on 8 deg cones with nose blowing (Figs. 7 and 8) are qualitatively similar to those observed on 12 deg cones; for example, on the 8 deg cone with $d_J = 1.0$ mm (Fig. 8), initially there is an increase in α_o from 18 deg (no jet flow) to 30 deg for $U_J/U_\infty = 1.0$, then a small decrease to 28 deg for $U_J/U_\infty = 1.24$ and 1.42 followed by an increase to 30 deg for higher velocity ratios. Similarly, the absolute maximum side force magnitudes have a variation with velocity ratio very similar to the 12 deg cone described previously. The features of vortex asymmetry onset and side force characteristics at higher Reynolds number will be discussed in a subsequent section.

It is interesting to observe that the previously described trends of α_o and maximum side force with jet velocity ratio are very similar to those observed with nose bluntness ratio [15]. We shall discuss these results further in Sec. III.J.

D. Effect of Nose Blowing on Vortex Asymmetry Onset

The results of vortex asymmetry onset as dependent on jet velocity ratio are further analyzed here. Results of α_o scaled by appropriate value of θ_C for each cone are shown plotted against velocity ratio U_J/U_∞ in Fig. 9. We shall first discuss the results on both the cone models at the lowest Re_D of 0.4×10^6. The results clearly show a collapse of data on each cone model, suggesting negligible influence of jet diameter d_J (within the limited variation of d_J examined here). Further, α_o/θ_C shows a nonmonotonic variation with jet velocity very similar to the results on nose blunting [15]. It is interesting to observe that there is a reasonably good collapse of the vortex asymmetry data up to a jet velocity ratio of about 0.7, beyond which there are differences for the two cone models. The α_o results corresponding to higher Reynolds number data (at Re_D of 0.9 and 5.4×10^6) are also shown in Fig. 9 and will be discussed later in Sec. III.H.

The aforementioned correlation of vortex asymmetry onset with the nose blowing shows dependence on two parameters, namely, the semicone angle (θ_C) and the jet velocity ratio (U_J/U_∞) and independent of Reynolds number (over a wide range of Re_D examined here). These observations suggest that inviscid flow mechanisms may play a dominant role in triggering vortex asymmetry even in the presence of nose blowing; similar observations have been made earlier with nose blunting as well as on the elliptic cones at high angles of attack (Rajan Kumar et al. [15] and Viswanath [27]).

E. Effect of Nose Blowing on Maximum Side Force Characteristics

The results of side force characteristics obtained on the two cone models at $Re_D = 0.4 \times 10^6$ have been further analyzed, and the absolute values of maximum side force generated on each cone model, as dependent on jet velocity ratio, are shown plotted in Fig. 10. The maximum side force levels decrease initially up to certain jet velocity ratio then a small increase followed by a gradual decrease for large values of velocity ratio. The results show a reasonably good collapse of the data at two values of d_J varied on each cone model. The trends for the two cone models are very similar, and the results show that the percentage decrease in side force levels due to blowing is nearly the same (about 80%) in both cases, which is a very significant indication of blowing effectiveness. Also, insensitivity of side force to jet diameter suggest that it is adequate to blow through a narrow hole to achieve the desired effectiveness and therefore lower mass and momentum requirements in applications.

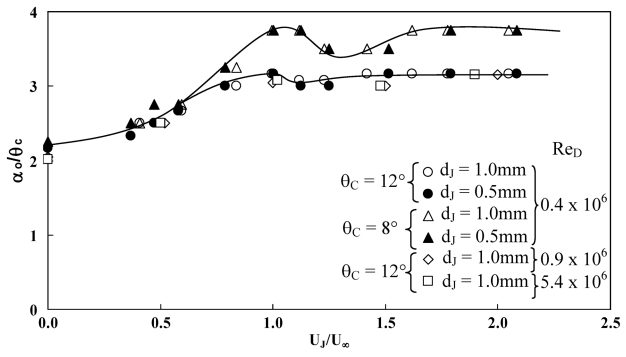

Fig. 9 Comparison of α_o characteristics for the two cone models with nose blowing.

F. Surface Pressure Distributions

We have noted the variation of maximum side force characteristics with jet velocity ratio for the two cone models (Fig. 10). Further support to the effectiveness of nose blowing may be seen by examining the measured surface pressure distributions on the 12 deg cone with $d_J = 0.5$ and 1.0 mm at $Re_D = 4 \times 10^5$. The results on 12 deg cone model with $d_J = 1.0$ mm at two longitudinal locations S1 and S2 (Fig. 2) at $U_J/U_\infty = 0.0$, 0.59, 0.99, 1.23, and 2.05 are presented in Figs. 11a–11e. The pressure distributions on the two sides (side *A* and side *B*, Fig. 2) with respect to the windward plane are plotted. It may be observed that nose blowing progressively symmetrizes the pressure distributions from the nose leading to reduction in side force levels generated; this may be seen by comparing pressure distributions at $U_J/U_\infty = 0.0$ and $U_J/U_\infty = 0.59$ (Figs. 11a and 11b). With increase in jet velocity ($U_J/U_\infty = 0.99$) the C_P distributions at both S1 and S2 become nearly symmetric (Fig. 11c) leading to very low side force levels (about 0.12) as observed in balance measurements (Fig. 10). At $U_J/U_\infty = 1.23$, a small degree of asymmetry at S2 location is evident (Fig. 11d), which, in fact, results in a weak second rise in side force (Fig. 10). At higher values of jet velocity ($U_J/U_\infty = 2.05$), the pressure distributions again become nearly symmetric at both S1 and S2 locations (Fig. 11e) leading to low levels of side force comparable to first minimum. The results of pressure distributions are broadly consistent with balance measurements presented earlier. Similar features of pressure distribution were reported [15] on side force control with nose blunting. The results of surface pressure distributions on 12 deg cone model with $d_J = 0.5$ mm showed features qualitatively very similar to those observed with $d_J = 1.0$ mm and are not included here (see [25]).

G. Surface Flow Features

We have already noted the variation of the absolute value of maximum side force with jet velocity ratio (Fig. 10). To gain a broad understanding of the vortex flow features, surface flow visualization studies using titanium dioxide in oil were carried out on 12 deg cone model with $d_J = 1.0$ mm at $\alpha = 40$ deg at different values of U_J and at $Re_D = 0.4 \times 10^6$. The surface flow patterns corresponding to

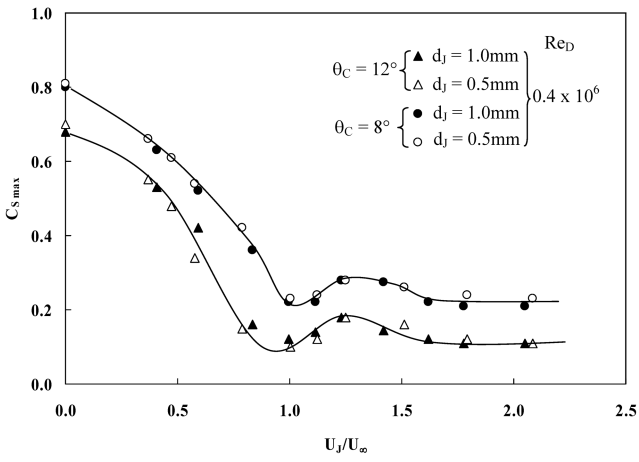

Fig. 10 Comparison of maximum side force characteristics for the two cone models with nose blowing.

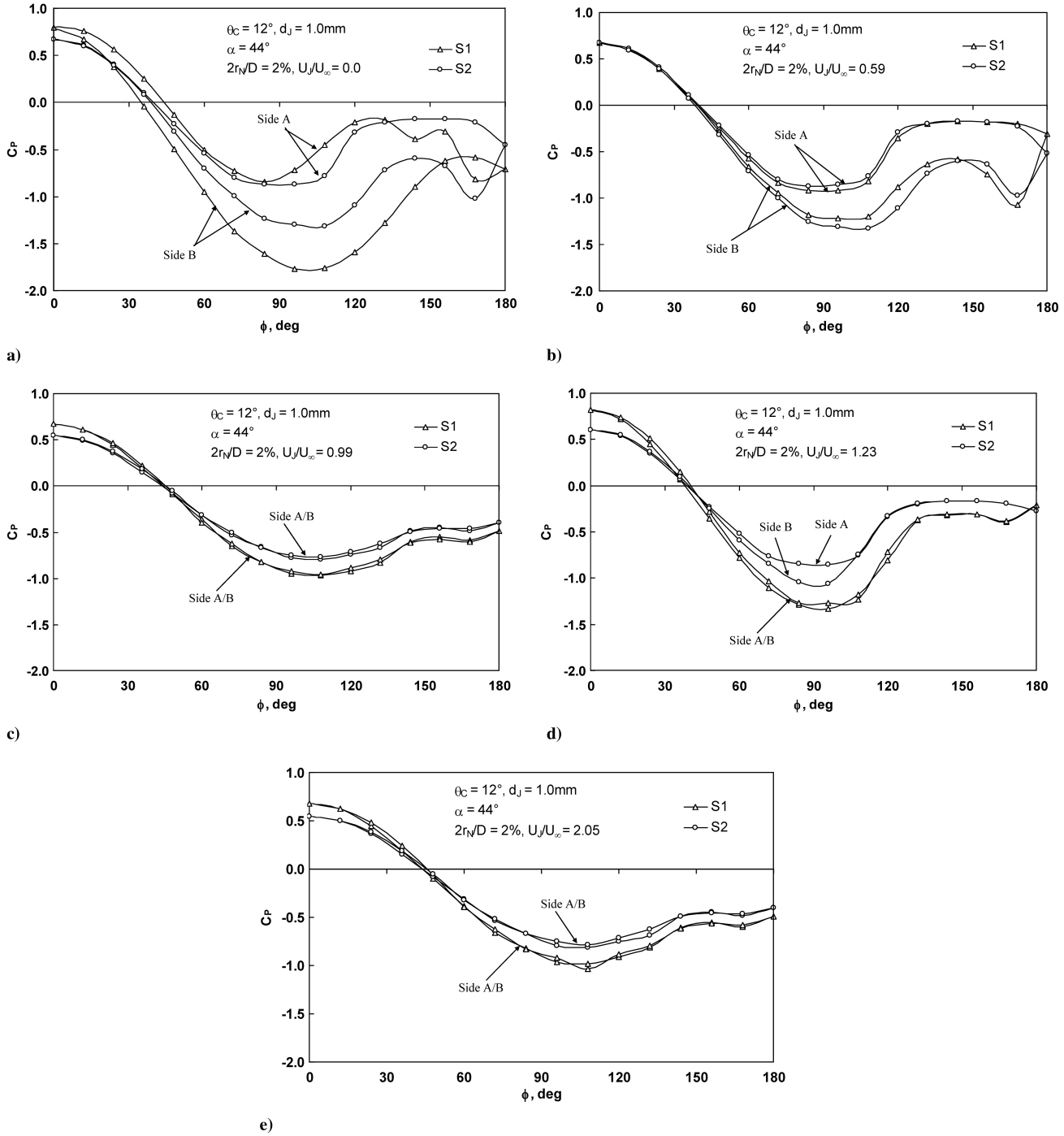

Fig. 11 Circumferential pressure distributions with nose blowing. a) $U_J/U_\infty = 0.0$; b) $U_J/U_\infty = 0.59$; c) $U_J/U_\infty = 0.99$; d) $U_J/U_\infty = 1.23$; e) $U_J/U_\infty = 2.05$.

$U_J/U_\infty = 0.0$ and 0.99 are presented in Fig. 12; also included are the crossflow topology interpreted from the surface flow features. In the absence of blowing, some degree of asymmetry in the primary and the secondary separation lines (SS1 and SS2, respectively) and primary reattachment (PR) may be noted (Fig. 12a); nearly symmetric features of the primary and the secondary separation are seen with blowing ($U_J/U_\infty = 1.0$, Fig. 12b), which resulted in lowest side force levels. Essentially, surface flow features show good visual consistency with side force levels generated.

H. Effect of Nose Blowing on Vortex Asymmetry Onset and Side Force Characteristics at High Reynolds Numbers

To characterize the effectiveness of the axial nose blowing, a large part of the measurements were made at $Re_D = 0.4 \times 10^6$, and the results of vortex asymmetry onset and side force characteristics have been discussed in detail in the previous sections. Limited force measurements on 12 deg cone model with $d_J = 1.0$ mm at $Re_D = 0.9$ and 5.4×10^6 were made to demonstrate the effectiveness of this novel technique at higher Reynolds numbers of relevance to practical applications. The results of vortex asymmetry onset at the higher Reynolds numbers are included in Fig. 9, along with the data at $Re_D = 0.4 \times 10^6$. It is very interesting to observe that the high Reynolds number data show good agreement with the onset results at $Re_D = 0.4 \times 10^6$.

The effect of Reynolds number on side force characteristics is shown in Fig. 13. The absolute value of maximum side force levels generated ($C_{S\max}$) at various values of U_J/U_∞ are normalized with maximum side force levels measured at $U_J/U_\infty = 0$ (C_{So}). The variations of $C_{S\max}/C_{So}$ with U_J/U_∞ at high Reynolds numbers ($Re_D = 0.9 \times 10^6$ and 5.4×10^6) are qualitatively similar to the data

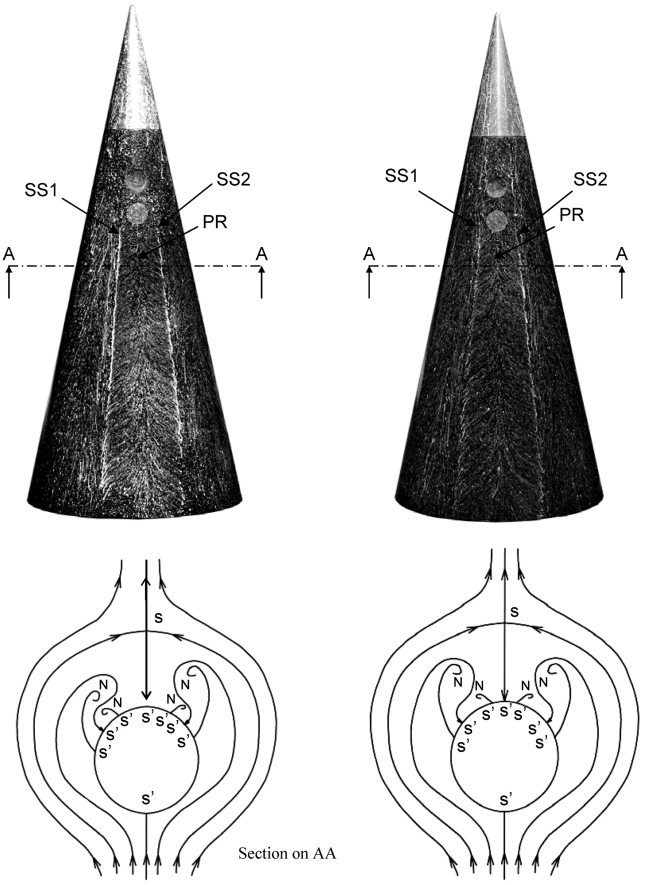

a) $U_J/U_\infty = 0.0$ **b) $U_J/U_\infty = 0.99$**

Fig. 12 Surface flow visualization photographs and crossflow streamlines on 12 deg cone model with nose blowing, $d_J = 1.0$ mm, $\alpha = 40$ deg (N, node; S, saddle; S′, half saddle), $Re_D = 0.4 \times 10^6$.

obtained at 0.4×10^6; the normalized side force initially decreases sharply with U_J/U_∞, reaches a minimum around $U_J/U_\infty = 1.0$, and shows a weak increase thereafter. The maximum reduction in side force levels is about 80% at $Re_D = 0.4 \times 10^6$, 65% at $Re_D = 0.9 \times 10^6$, and 55% at $Re_D = 5.4 \times 10^6$. These results are considered very significant as they demonstrate the effectiveness of axial nose blowing over a wide range of Reynolds numbers of interest in engineering designs.

I. Blowing Mass and Momentum Requirements for Side Force Control

We have seen in the earlier discussion that the jet velocity ratio U_J/U_∞ is a very useful parameter characterizing jet effectiveness. From the application point of view, it is important to estimate the jet mass and momentum requirements for side force control. To do this, we use a normalized mass and momentum parameter of jet as defined below:

$$\text{jet mass ratio}, \qquad C_m = \frac{m_j}{m_\infty} = \frac{\rho_j U_j A_j}{\rho_\infty U_\infty A_b}$$

$$\text{jet momentum ratio}, \qquad C_\mu = \frac{m_J U_j}{m_\infty U_\infty}$$

The variation of maximum side force characteristics with the estimated values of C_m and C_μ for the 8 and 12 deg cone models (with $d_J = 1.0$ mm) at various Reynolds numbers tested are shown in Figs. 14 and 15, respectively. The general trend of side force characteristics with C_m and C_μ are very similar to those observed with jet velocity ratio U_J/U_∞, which is to be expected. As may be evident, the mass and momentum required corresponding to the first

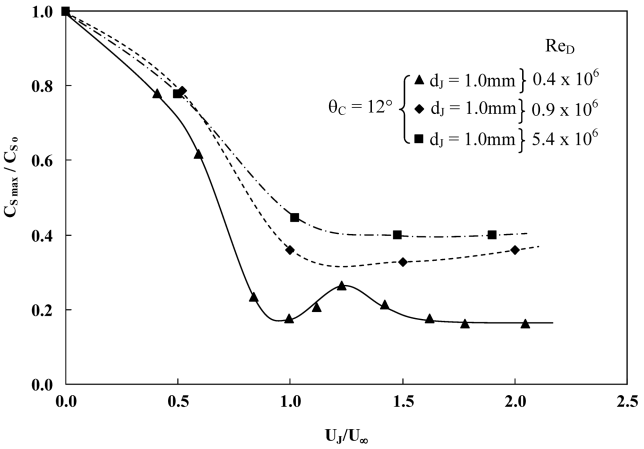

Fig. 13 Effect of Reynolds number on maximum side force characteristics.

minimum in side force are indeed very small and nearly independent of Reynolds number over the range of Reynolds numbers tested.

J. Possible Flow Mechanisms Associated with Nose Blowing for Side Force Control

In the preceding sections, we have presented results demonstrating the effectiveness of axial nose blowing for control of side forces on two cone models. Many similarities between axial nose blowing and nose blunting [15] have been observed, in particular, with regard to the reduction of maximum side forces and associated changes in α_o characteristics. The most spectacular feature is the observed trend of maximum side force variation with jet velocity ratio U_J/U_∞, including the smaller second peak in side force characteristics (Fig. 10), which bears strong similarity with nose bluntness effects (Fig. 16, reproduced from [15]). Also, the data generated here at low speeds indicate that jet velocity ratio is the appropriate parameter governing effectiveness of nose blowing (Figs. 9 and 10). These observations strongly suggest that flow mechanisms associated with nose blowing may have certain broad similarities with those of nose blunting. An explanation based on inviscid flow considerations is attempted here.

We may, therefore, expect that, on the vertical plane of symmetry, an important feature is the interaction of the jet velocity U_J, with the component of the freestream velocity along the jet flow axis $U_\infty \cos\alpha$ (Fig. 17); such an interaction would result in a stagnation point (S) ahead of the nose apex as depicted schematically in Fig. 17. Depending on the value of U_J/U_∞, the location of the stagnation point would vary; for example, if U_J/U_∞ is large, the stagnation point would move away from the nose apex and vice versa. Also, the physical scale of the oncoming flow influenced or perturbed by the formation of a stagnation point may be expected to increase with

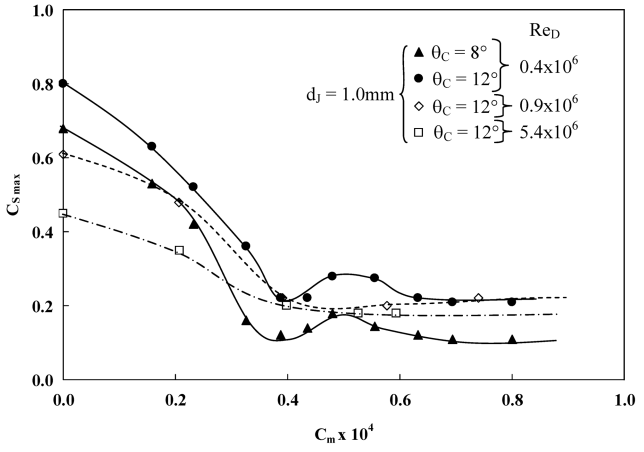

Fig. 14 Variation of maximum side force characteristics with jet mass flow ratio.

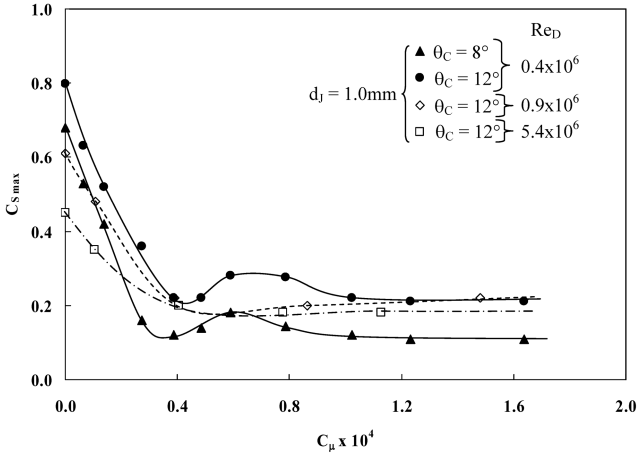

Fig. 15 Variation of maximum side force characteristics with jet momentum ratio.

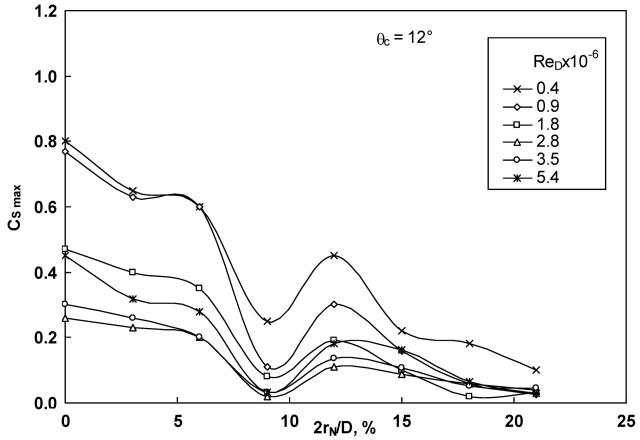

Fig. 16 Variation of maximum side force characteristics with bluntness ratio (taken from [15]).

U_J/U_∞ and vice versa. In essence, nose blowing may be affecting the freestream flow by the formation of what we may call "fluid dynamic blunting," whose effects will primarily depend on U_J/U_∞; in other words, the undisturbed freestream flow will respond to the fluid dynamic blunting effects and perhaps not see the presence of the sharp cone. Calculations of the upstream flowfield with blowing using inviscid momentum equations may throw more light onto the broad explanation suggested here.

K. Normal Force Characteristics

As indicated earlier, the focus in these tests being on vortex asymmetry onset and side force characteristics with nose blowing, which has been presented in great detail, we show here limited results on normal force characteristics for certain cases for completeness. Typical results on the 8 and 12 deg cone models with $d_J = 1.0$ mm at a few selected values of jet velocity are presented in Figs. 18 and 19, respectively. The slope of the normal force curve given by the slender body theory (=2.0, valid for large slenderness ratios) is also shown in Figs. 18 and 19 for a broad comparison. It is interesting to observe that the normal force characteristics (for both the cones with and without nose blowing) in the linear range ($\alpha \leq 10$ deg) show broad consistency with the slender body results; further, nonlinear effects at higher α (≥ 20 deg) arising from the vortex flows may be observed. A reduction in the values of $C_{N\max}$ of about 4 and 12% for the 8 and 12 deg cone models, respectively, is observed with nose blowing ($U_J/U_\infty = 2.05$) at $\alpha = 45$ deg; this reduction is possibly associated with the altered flowfield and significantly lower level of side force generated due to nose blowing.

IV. Conclusions

The effect of axial nose blowing against oncoming flow for side force control on two slender cone models has been investigated at low speeds; this is possibly the first time such an active control methodology involving nose blowing has been explored. The tests were made on the 8 and 12 deg cone models with (circular) jet flow at several jet velocity ratios; while a large body of the data on nose blowing effectiveness was generated at a $Re_D = 0.4 \times 10^6$, limited high Reynolds number (0.9×10^6 and 5.4×10^6) experiments were carried out as well to assess its effectiveness relevant to real practical applications.

Nose blowing was found to be very effective in lowering the max side forces generated over a wide range of Reynolds numbers; the (maximum) side force reductions observed were in the range of 55–80%, depending on the test Reynolds number. The jet velocity ratio was found to be the relevant parameter for characterizing the jet effectiveness for side force control.

The absolute value of maximum side force levels decreased gradually up to a certain jet velocity ratio (around 1.0), then a small increase followed by a gradual decrease for large values of velocity ratio; this decrease or increase in side force levels with nose blowing was associated with a corresponding increase or decrease, respectively, in the onset of vortex asymmetry. The results showed a negligible influence of jet diameter on the vortex asymmetry onset and maximum side force characteristics (within the limited variation of jet diameter varied in these tests).

The correlation of angle of attack for vortex asymmetry onset with nose blowing was found to be virtually independent of Reynolds

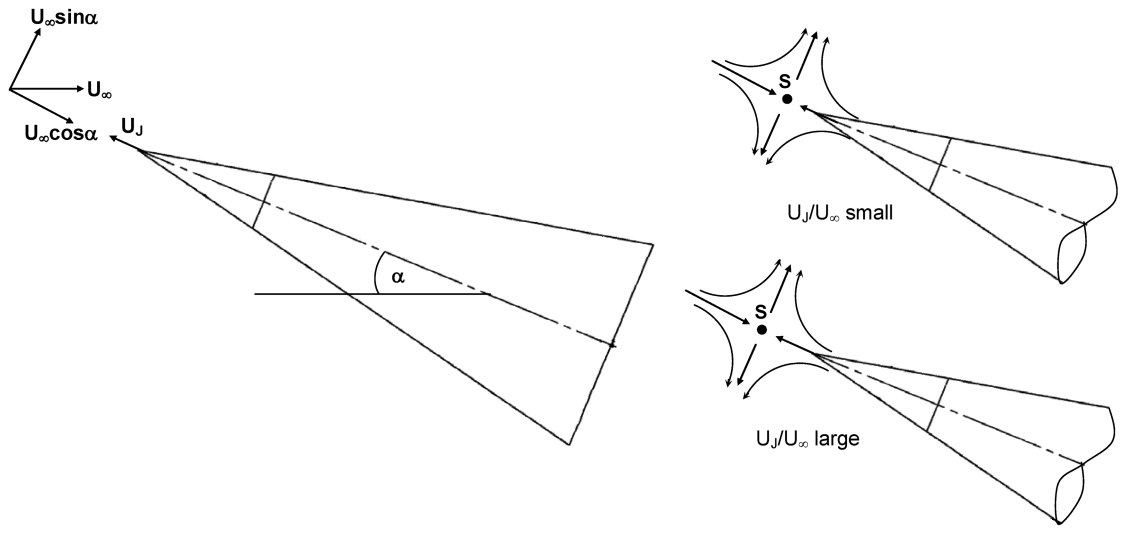

Fig. 17 A schematic of possible flow mechanisms associated with nose blowing.

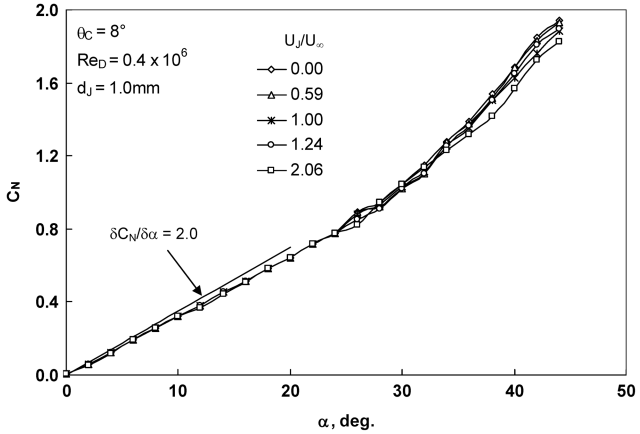

Fig. 18 Normal force characteristics on 8 deg cone model with nose blowing.

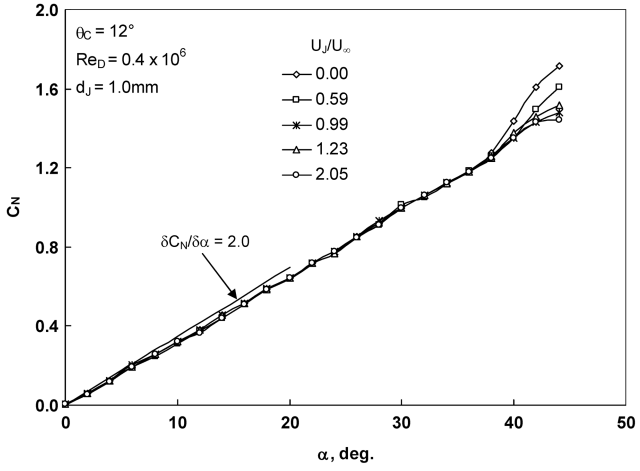

Fig. 19 Normal force characteristics on 12 deg cone model with nose blowing.

number and depended essentially on the geometrical model parameter θ_C and the jet velocity ratio; these observations support the view that the inviscid flow mechanisms may play a dominant role in triggering vortex asymmetry on slender cones in the presence of nose blowing as well, similar to those observed on experiments with nose blunting. The many similarities in the results of vortex asymmetry onset and maximum side force characteristics generated between nose blowing and nose blunting [15] suggest that nose blowing may result in some kind of fluid dynamic blunting ahead of the nose apex essentially by the interaction of the freestream flow with the injected jet from the nose.

Acknowledgments

The authors sincerely thank the Aeronautical Development and Research Board, Government of India, for their financial assistance to carry out this work. We would also like to thank the Director of the National Aerospace Laboratories and the Head of National Trisonic Aerodynamic Facilities for providing facilities to conduct this research work. Thanks are due to the staff of the 1.2 m trisonic wind tunnel and the 1.5 m low speed wind tunnel for their valuable help during wind-tunnel testing.

References

[1] Hunt, B. L., "Asymmetric Vortex Forces and Wakes on Slender Bodies," AIAA Paper 82-1336, Aug. 1982.

[2] Ericsson, L. E., and Reding, J. P., "Asymmetric Flow Separation and Vortex Shedding on Bodies of Revolution," *Progress in Astronautics and Aeronautics*, AIAA, Washington DC, 1989, pp. 391–452.

[3] Champigny, P., "Side Forces at High Angles of Attack. Why, When, How?," *29th AAAF Symposium on Applied Aerodynamics*, Biscarosse, France, 1992.

[4] Williams, D. R., "A Review of Forebody Vortex Control Scenarios," AIAA Paper 97-1967, Feb. 1997.

[5] Coe, P. L., Chambers, J. R., and Letko, W., "Asymmetric Lateral-Directional Characteristics of Pointed Bodies of Revolution at High Angles of Attack," NASA TN D-7095, 1972.

[6] Keener, E. R., and Chapman, G. T., "Onset of Aerodynamic Side Forces at Zero Sideslip on Symmetric Forebodies at High Angles of Attack," AIAA Paper 74-770, 1974.

[7] Modi, V. J., Cheng, C. W., Mak, A., and Yokomizo, T., "Reduction of the Side Force on Pointed Forebodies Through Add-On Tip Devices," *AIAA Journal*, Vol. 30, No. 10, 1992, pp. 2462–2468.

[8] Howard, R. M., and Yuan, C. C., "Effect of Forebody Strakes on Missile Asymmetric Vortices," *Journal of Spacecraft and Rockets*, Vol. 28, No. 4, 1991, pp. 411–417.

[9] Ng, Y. T., Luo, S. C., and Lim, T. T., "Effect of Strake Position on the Flow past an Inclined Ogive Cylinder," *AIAA Journal*, Vol. 42, No. 2, 2004, pp. 418–419. doi:10.2514/1.861

[10] Letko, W., "A Low-Speed Experimental Study of the Directional Characteristics of a Sharp-Nosed Fuselage Through a Large Angle-of-Attack Range at Zero Angle of Sideslip," NACA TN 2911, 1953.

[11] Rao, D. M., "Side Force Alleviation on Slender Pointed Forebodies at High Angles of Attack," *Journal of Aircraft*, Vol. 16, 1979, pp. 763–768.

[12] Pick, G. S., "Investigation of Side Forces on Ogive-Cylinder Bodies at High Angles of Attack in the $M = 0.5$ to 1.1 Range," AIAA Paper 71-570, June 1971.

[13] Chapman, G. T., Keener, E. R., and Malcolm, G., "Asymmetric Aerodynamic Forces on Aircraft Forebodies at High Angles of Attack: Some Design Guides," AGARD Paper 16, 1976.

[14] Fidler, J. E., "Active Control of Asymmetric Vortex Effects," AIAA Paper 80-0182, Jan. 1980.

[15] Rajan Kumar, Viswanath, P. R., and Ramesh, O. N., "Nose Bluntness for Side Force Control on Circular Cones at High Incidence," *Journal of Aircraft*, Vol. 42, No. 5, 2005, pp. 1133–1141. doi:10.2514/1.10292

[16] Williams, D. R., and Papazian, H., "Forebody Vortex Control with the Unsteady Bleed Technique," *AIAA Journal*, Vol. 29, No. 5, 1991, pp. 853–855.

[17] Bernhardt, J., and Williams, D. R., "The Effect of Reynolds Number on Control of Forebody Asymmetry by Suction and Bleed," AIAA Paper 93-3265, July 1993.

[18] Bernhardt, J., and Williams, D. R., "Proportional Control of Asymmetric Forebody Vortices," *AIAA Journal*, Vol. 36, No. 11, 1998, pp. 2087–2093.

[19] Degani, D., and Tobak, M., "Experimental Study of Controlled Tip Disturbance Effect on Flow Asymmetry," *Physics of Fluids A*, Vol. 4, No. 12, Dec. 1992, pp. 2825–2832. doi:10.1063/1.858338

[20] Skow, A. M., Moore, W. A., and Lorincz, D. J., *Forebody Vortex Blowing: A Novel Concept to Enhance the Departure/Spin Recovery Characteristics of Fighter Aircraft*, AGARD, Paper CP-262, 1979.

[21] Malcolm, G. N., Ng, T. T., "Forebody Vortex Manipulation for Aerodynamic Control of Aircraft at High Angles of Attack," SAE Paper 89-2220, 1989.

[22] Roos, F. W., and Magness, C. L., "Bluntness and Blowing for Flowfield Asymmetry Control on Slender Forebodies," AIAA Paper 93-3409, Aug. 1993.

[23] Roos, F. W., "Microblowing for High-Angle-of-Attack Vortex Flow Control on a Fighter Aircraft," *Journal of Aircraft*, Vol. 38, No. 3, 2001, pp. 454–457.

[24] Malcolm, G. N., "Forebody Vortex Control," *Progress in Aerospace Sciences*, Vol. 28, No. 11, 1991, pp. 171–234. doi:10.1016/0376-0421(91)90005-O

[25] Rajan Kumar, "Experimental Study of Side Force Control on Slender Cones at High Angles of Attack," Ph.D. Dissertation, Department of Aerospace Engineering, Indian Institute of Science, Bangalore, India, 2005.

[26] Kline, S. J., and McClintock, F. A., "Describing Uncertainties in Single-Sample Experiments," *Mechanical Engineering*, Vol. 75, 1953, pp. 3–8.

[27] Viswanath, P. R., "Vortex Asymmetry and Induced Side Forces on Elliptic Cones at High Incidence," *Journal of Aircraft*, Vol. 32, No. 5, 1995, pp. 1018–1025.